LAND SURFACE MICROWAVE EMISSIVITIES OVER THE GLOBE FOR A DECADE

by Catherine Prigent, Filipe Aires, and William B. Rossow

A global, decade-long microwave land surface emissivity dataset calculated from SSM/I satellite observations between 19 and 85 GHz is available to the community and possible applications are illustrated.

Passive microwave observations from satellites have long been used over the ocean to estimate atmospheric properties such as water vapor, temperature profiles, or cloud liquid water paths. They have not been fully exploited over land, because of the large and variable contribution of the land surface to the upwelling radiation. The passive microwave signal emerging from the surface is sensitive to many surface parameters such as the vegetation cover, the soil moisture, the surface roughness, or the presence of standing water or snow, in addition to depending upon frequency, incidence angle, and polarization. All these surface characteristics interact with the microwave radiation in ways that are complex to model, being dependent on a large number of highly variable and poorly known parameters. Efforts have been made to better understand the microwave radiative transfer at the surface from theoretical calculations and from measurements. In addition to model developments, adjoint models are also generated in the framework of variational data assimilation (Jones et al. 2004). Even assuming that a perfect land surface emissivity model existed, the inputs it would require (e.g., vegetation parameters, soil moisture, surface roughness) are not sufficiently known on a global basis with the adequate spatial resolution and with the required accuracy. Likewise, retrieving these parameters from microwave radiances requires a theoretical model that is questionable, especially for vegetated regions.

Very few groups have examined the problem of microwave land surface emissivities at a global scale. Weng et al. (2001) or Pellerin et al. (2003) choose to

AFFILIATIONS: Prigent—Centre National de la Recherche Scientifique, Laboratoire d'Etudes du Rayonnement et de la Matière en Astrophysique, Observatoire de Paris, Paris, France; Aires—Centre National de la Recherche Scientifique/L'Institut Pierre-Simon Laplace, Laboratoire de Météorologie Dynamique, University Paris VI, Paris, France; Rossow—NASA Goddard Institute for Space Studies, New York, New York.
CORRESPONDING AUTHOR: Dr. Catherine Prigent, Centre National de la Recherche Scientifique, Laboratoire d'Etudes du Rayonnement et de la Matière en Astrophysique, Observatoire de Paris, 61, avenue de l'Observatoire, Paris, France
E-mail: Catherine.Prigent@obspm.fr

develop a global model to estimate the emissivity for the various surface conditions encountered over the continents, using different radiative transfer solutions depending on the surface characteristics. Inputs for the radiative transfer model can be provided by a land surface model, such as the Global Land Data Assimilation System (Rodell et al. 2004). In contrast, global land surface emissivities are produced at Special Sensor Microwave Imager (SSM/I) frequencies by Prigent et al. (1997, 1998), directly from the satellite observations, by removing the contribution of the atmosphere, clouds, rain, and the surface temperature using ancillary data. The emissivities are estimated for SSM/I observation conditions (i.e., for a 53° zenith angle at 19.35, 22.235, 37.0, and 85.5 GHz for both orthogonal polarizations). The Advanced Microwave Sounder Units (AMSU) emissivities have also been calculated (Prigent et al. 2005a; Karbou et al. 2005a).

Microwave land surface emissivities can be used for several purposes including land surface characterization and atmospheric retrieval over land from satellite passive microwave observations. Estimates of these emissivities are particularly important today as the major Numerical Weather Prediction (NWP) centers are currently attempting to assimilate passive microwave observations over land.

The objective of this paper is to describe a technique to calculate the microwave emissivity from satellite measurements and in particular to present the global decade-long emissivity dataset derived from SSM/I observations between 19 and 85 GHz and its sensitivity to land surface properties. Uses of these emissivities are listed in the conclusions.

EMISSIVITY CALCULATION FROM SATELLITE OBSERVATIONS.
In this study, the microwave satellite observations are derived from the SSM/I instruments on board the Defense Meteorological Satellite Program (DMSP) polar satellites. They observe the Earth twice daily at 19.35, 22.235, 37.0, and 85.5 GHz with both vertical and horizontal polarizations, with the exception of 22 GHz, which is for vertical polarization only. The observing incident angle is close to 53°, and the elliptical fields of view decrease in size proportionally with frequency, from 43×69 to 13×15 km^2. Intersensor calibration was examined by Colton and Poe (1999) and showed limited differences from sensor to sensor. The emissivity calculation method is fully described in Prigent et al. (1997, 1998) and is summarized here.

Over a flat, lossy surface, the integrated radiative transfer equation in the Rayleigh–Jeans approximation for a nonscattering plane-parallel atmosphere can be written as

$$\text{Tb}_p = T_{\text{surf}} \varepsilon_p e^{-\tau(0,H)/\mu} \quad (1)$$
$$+ T_{\text{atm}}^{\downarrow}(1-\varepsilon_p)e^{-\tau(0,H)/\mu} + T_{\text{atm}}^{\uparrow},$$

with

$$T_{\text{atm}}^{\downarrow} = \int_H^0 T(z)[\alpha(z)/\mu]e^{-\tau(z,0)/\mu}dz + T_{\text{cosm}}e^{-\tau(0,H)/\mu}$$

and

$$T_{\text{atm}}^{\uparrow} = \int_0^H T(z)[\alpha(z)/\mu]e^{-\tau(z,H)/\mu}dz.$$

Here Tb_p is the brightness temperature measured by the satellite for polarization p; T_{surf} is the physical surface "skin" temperature; ε_p is the surface emissivity for polarization p; $\mu = \cos(\theta)$, with θ being the incidence angle on the surface; $\alpha(z)$ is the atmospheric absorption at altitude z; $T(z)$ is the atmospheric temperature at altitude z;

$$\tau(z_0, z_1) = \int_{z_0}^{z_1} \alpha(z)dz$$

is the atmospheric extinction from z_0 to z_1; H is the orbiter height; and T_{cosm} is the cosmic background brightness temperature.

This leads to

$$\varepsilon_p = \frac{\text{Tb}_p - T_{\text{atm}}^{\uparrow} - T_{\text{atm}}^{\downarrow}e^{-\tau(0,H)/\mu}}{e^{-\tau(0,H)/\mu}(T_{\text{surf}} - T_{\text{atm}}^{\downarrow})}. \quad (2)$$

Note that with increasing opacity at the observed frequency, the surface contribution to the measured signal Tb_p decreases and the error in ε_p increases.

At frequencies above ~19 GHz, the radiation is expected to emanate from only a thin surface layer with a penetration depth of the order of the wavelength. If there is no volume scattering, the surface temperature is the actual skin temperature, and for flat surfaces the reflection is quasi specular; in these conditions, Eqs. (1) and (2) are strictly valid. However, volume scattering can be involved over very dry sands, deep vegetation canopies, or significant snow layers. Microwave penetration in sand deserts has been analyzed carefully in Prigent et al. (1999), using a coincident diurnal cycle of IR-derived surface skin temperature and SSM/I observations. It shows that in sand dunes, penetration depth can be as large as five wavelengths. In these cases, Eq. (2) is not valid, especially at low frequency, and in our emissivity climatology these areas are flagged.

In addition, when the terrain is rough on scales between the radiation wavelength and the size of the field of view, the surface is no longer specular

and surface scattering is present. Questions about the validity of the specular approximation were raised (Matzler 2005). Karbou and Prigent (2005) quantified the error introduced by this approximation and concluded that, especially at the 53° incidence angle, the impact of a specular assumption is very limited, even over rather rough surfaces. In most cases Eqs. (1) and (2) involve some "effective" emissivity and temperature, aggregated over the depth of penetration and the field of view of the instrument.

The method consists in solving the radiative transfer Eq. (2) for the effective surface emissivity for each channel using ancillary data to specify the atmospheric and other surface parameters. For simplicity in the following, the term effective is omitted. Ancillary data are provided by the International Satellite Cloud Climatology Project (ISCCP; Rossow and Schiffer 1999) and the National Centers for Environmental Prediction–National Center for Atmospheric Research (NCEP–NCAR) reanalyses (Kalnay et al. 1996). The satellite observations and the ancillary data are all gridded on a 0.25° × 0.25° equal-area grid that is compatible with both the SSM/I and ISCCP spatial sampling.

Cloud-free SSM/I observations are first isolated using collocated visible/infrared satellite observations (ISCCP data). For a given SSM/I observation, the two 3-hourly ISCCP estimates that bracket the SSM/I overpass time are checked. There is no evidence of cloud contamination in the resulting emissivity calculation. The cloud-free atmospheric contribution is then calculated using a radiative transfer model and an estimate of the atmospheric temperature–humidity profile from the NCEP–NCAR reanalysis. Finally, with the surface skin temperature derived from IR observations (interpolated from the two 3-hourly ISCCP estimates that bracket the SSM/I overpass), the surface emissivity is calculated for all seven SSM/I channels. An IR emissivity of 1 is assumed in the original ISCCP T_{surf}, but a correction is applied to account for the IR emissivity variations with surface types [similar to Ruston and Vonder Haar (2004) in their microwave emissivity calculation from SSM/I over the United States during summertime]. Figure 1 summarizes the different steps in the
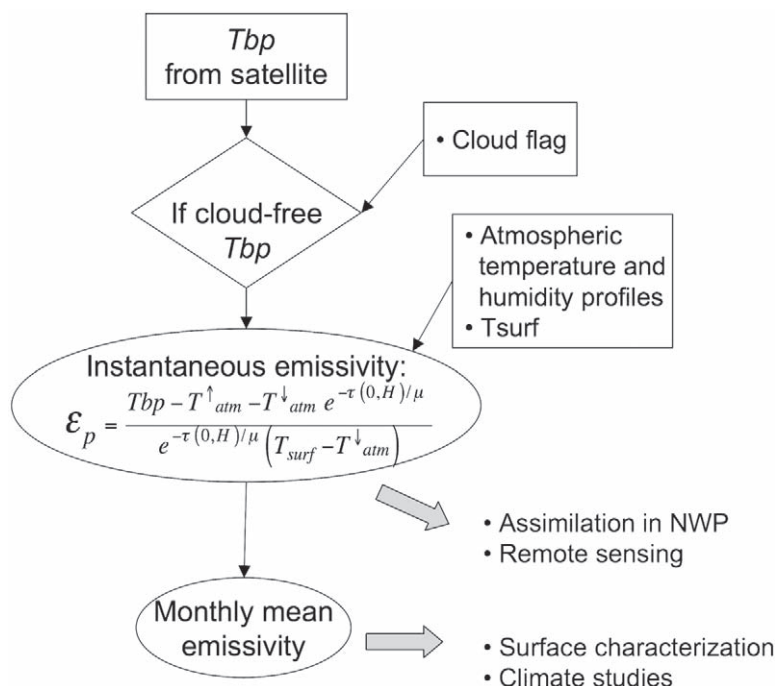
Fig. 1. Land surface emissivity calculation derived from satellite observations. The different steps.

emissivity calculation. An emissivity error analysis was conducted (Prigent et al. 1997) by examining each source of errors in the calculation process; the accuracy of the instantaneous retrieved emissivities is estimated to be within 1%–2%.

Instantaneous microwave emissivities can be used directly for remote sensing application (Fig. 1) or assimilation in NWP. In order to have complete emissivity coverage over land, the emissivity calculations are averaged over time. What is the optimum averaging period? Figure 2 shows the mean number of clear pixels obtained for the SSM/I satellites (*F-10* and *F-11*) during 5, 10, and 30 days in January and July 1994, versus the latitude, along with the corresponding portion of land covered for the same periods of time. Especially in the intertropical zone where the cloud cover can be persistent, averaging over a long time is necessary to reach good coverage. Figure 3 presents the frequency distribution of the emissivity standard deviations at 19-GHz horizontal polarization over the same three time periods for the same months. With increasing time period, the mode of the emissivity standard deviation increases due to emissivity variations at a given location with changing surface properties (e.g., soil moisture, vegetation phenology, etc.). The increase in emissivity variability is especially clear in winter because of the presence of snow, which induces significant emissivity changes.

GLOBAL MONTHLY MEAN MICROWAVE EMISSIVITIES AND THEIR SENSITIVITY TO SURFACE CHARACTERISTICS. *Global emissivity characteristics.* Microwave responses to the land surface include contributions from the soil, from the vegetation, and occasionally from standing water or snow. Extensive efforts have been directed toward a better understanding of the mechanisms responsible for the microwave emission from each factor, both from theoretical analysis (e.g., Shi et al. 2002) and from field experiments [e.g., Wigneron et al. (1997) and Hewison (2001) from aircraft instruments].

Figure 4 shows the global maps of monthly mean 37-GHz emissivities for horizontal polarization and for the polarization difference [vertical (V) minus horizontal (H)] for January and July 2001, as derived from SSM/I observations.

The bare soil response depends on soil dielectric properties and roughness. The soil dielectric properties are essentially sensitive to the soil moisture, given the large contrast between the high dielectric constant of water as compared to the soil. Different roughness scales interfere with the signal, from the small-scale roughness (cf. the wavelength) to the large topographic roughness and terrain slopes

(hills, mountains, etc.). Smooth bare soils have a quasi-specular reflection, producing high polarization emissivity differences around 53° incidence. In Fig. 4, rather flat, arid bare surfaces (e.g., northern Africa, the Arabian Peninsula) are associated with low emissivities at horizontal polarization and high polarization differences as compared to surrounding vegetated areas. When the terrain gets rougher, surface scattering causes the emissivity polarization difference to decrease. Over mountain areas (the Tibesti in Chad or the Ahaggar Mountain in Algeria, e.g., for instance in Fig. 4), the polarization difference decreases, related to the scattering induced by the topographic roughness.

Vegetation absorbs, emits, and scatters microwave radiation; its radiative properties are mainly controlled by the dielectric properties of vegetation components, their density, and the relative size of vegetation components with respect to the wavelength. Increasing vegetation density increases the emissivity in horizontal polarization and reduces the emissivity polarization difference. As expected, densely vegetated zones (e.g., the tropical rainforest in Africa or in South America in Fig. 4) exhibit high emissivities at horizontal polarization and low polarization differences. The gradient below 15°N in Africa corresponds to the bush and sparse-vegetation transition region between the Sahara and the rainforest and, as expected, this region is broader in winter than in summer.

Open-water surfaces (lakes, rivers, and inundated areas) produce very low emissivities in both horizontal and vertical polarizations along with a high polarization difference. As a consequence, the major river systems (e.g., the Mississippi River basin in the United States, the Amazon in South America, or the Ob in Russia), large wetlands, and lakes appear clearly on the emissivity maps. Given the spatial resolution of the SSM/I instrument, small rivers and lakes are averaged out and cannot be detected on the emissivity maps.
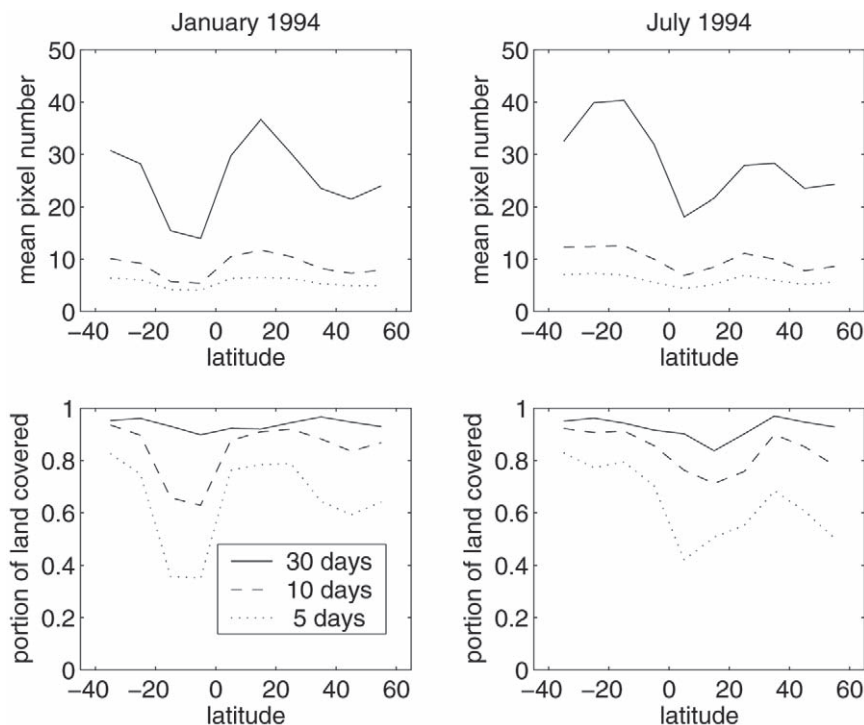
FIG. 2. For (left) January and (right) July 1994 the mean number of clear pixels observed by the SSM/I satellites (*F-10* and *F-11*) during (top) 5, 10, and 30 days and (bottom) the corresponding portion of land covered for the same periods of time versus the latitude.
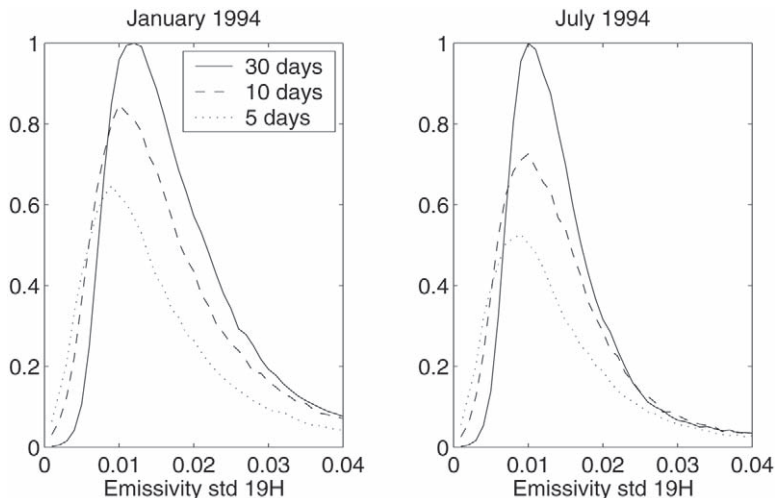
FIG. 3. Normalized histograms of the emissivity standard deviation at 19-GHz horizontal polarization over 5, 10, and 30 days for (left) January and (right) July 1994. For each month, the histograms are normalized by the maximum of the monthly values.

Maps at 19 and 85 GHz present very similar spatial structures and temporal variations (not shown). For more details on the frequency dependence of the emissivities see Prigent et al. (2000, 2005a). Note that the brightness temperature polarization difference at a given frequency, as directly measured by the instrument, or the Microwave Polarization Difference index (the brightness temperature polarization difference over their sum) also shows sensitivity to the vegetation, soil moisture, or the presence of standing water (e.g., Choudhury 1990; Owe et al. 2001). However, these quantities are modulated by the atmospheric contribution and by the surface temperature and as a consequence are not solely sensitive to the surface characteristics.

Sensitivity of the emissivities to vegetation and surface soil moisture. Because passive microwave emissivities are sensitive to both vegetation and soil moisture, studies tend to isolate the two sources of variability in order to retrieve the soil moisture (e.g., Lakshmi et al. 1997; Vinnikov et al. 1999; de Ridder 2003). Figure 5 presents a Hovmöller graph of the emissivity polarization difference at 37 GHz for 8 yr in Africa between 6° and 16°N at 20°E in the transition zone between vegetated regions and deserts. For each year a strong seasonal cycle is present north of 7°, with a minimum in the emissivity difference in summer, related to the maximum vegetation density. In addition, a significant interannual variability is observed, with a minimum in the emissivity difference (lower than
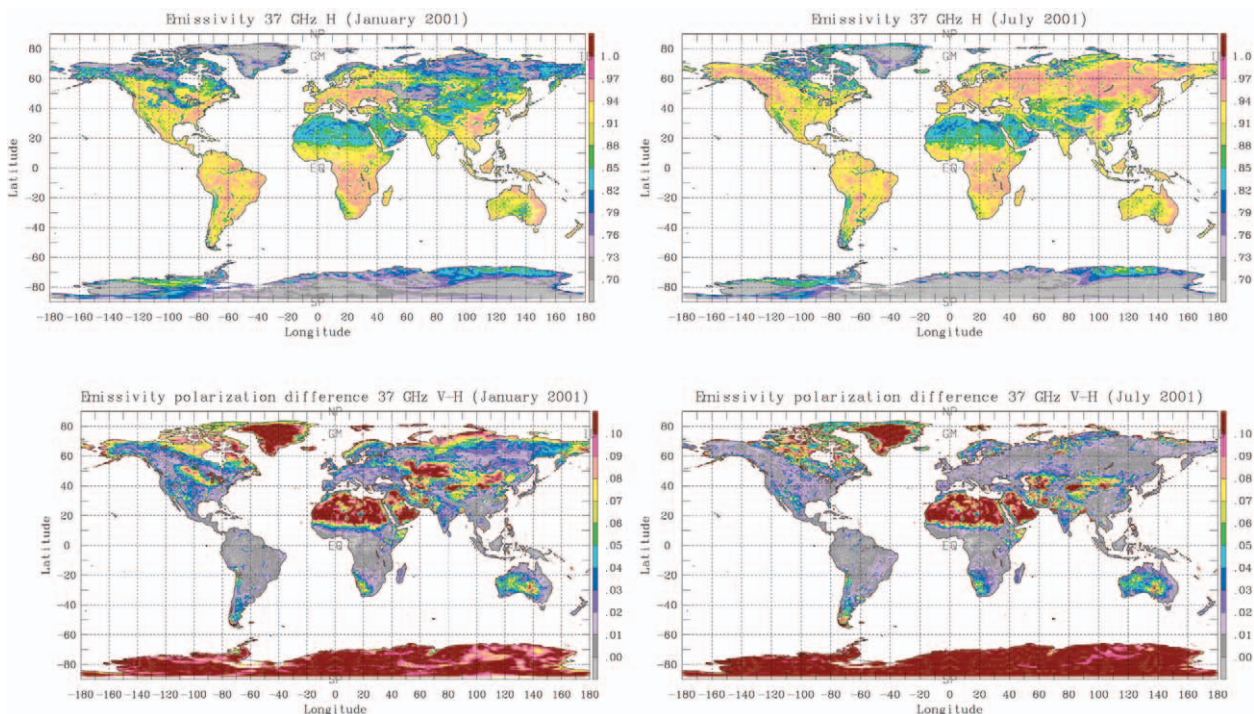

FIG. 4. Global maps of monthly mean 37-GHz emissivities, as derived from SSM/I observations, for (top) horizontal polarization and (bottom) for the polarization difference (V – H) for (left) January and (right) July 2001.
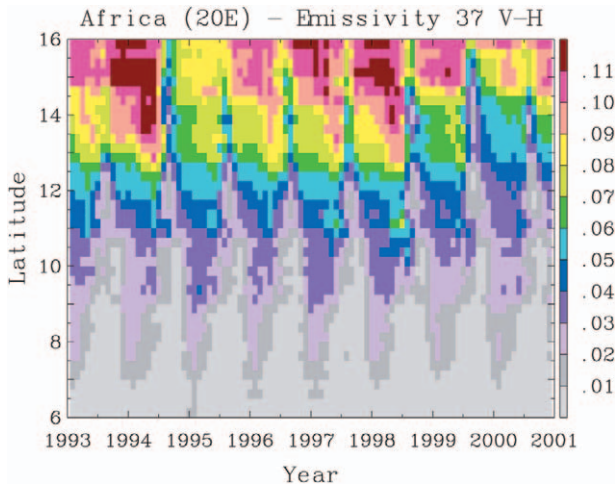
Fig. 5. Hovmöller graph of the emissivity polarization difference (V – H) at 37 GHz, for 8 yr in Africa between 6° and 16°N at 20°E.

0.03) in 1994 and 1999 around 14°N. How do these seasonal and interannual cycles relate quantitatively to the vegetation density and to the soil moisture?

In order to examine the relationship between the emissivities and the vegetation more closely, the Normalized Difference Vegetation Index (NDVI) derived from the visible and near-infrared Advanced
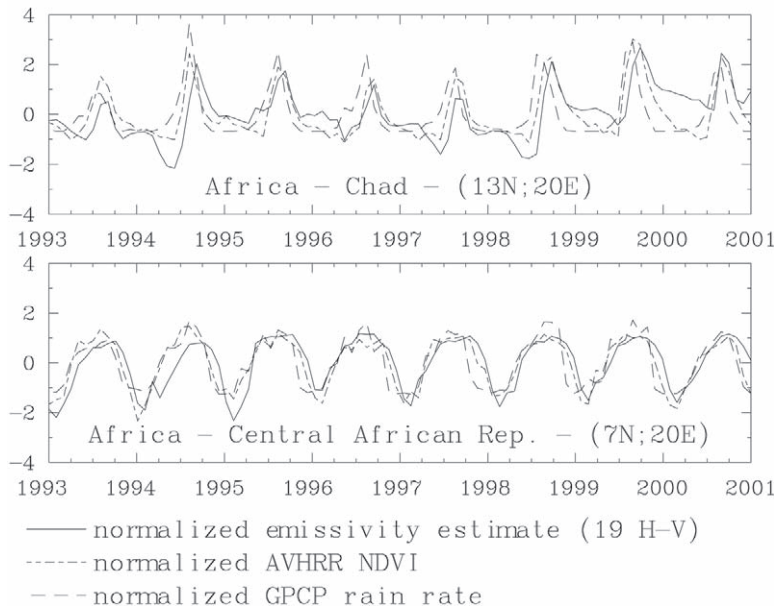

Fig. 6. The 8-yr time series of normalized values (subtracting the mean and dividing by the standard deviation) of the emissivity polarization difference at 19 GHz, the AVHRR NDVI, and the GPCP rain rate for two locations along the previous transect, at 7° and at 13°N. Note that the difference in emissivity between horizontal and vertical polarization is presented, not the opposite as usual, in order to have a positive correlation with the other variables and an easier comparison.

Very High Resolution Radiometer (AVHRR) observations on the National Oceanic and Atmospheric Administration (NOAA) polar-orbiting environmental satellites has been collected for the same period of time; this index has been shown to be related to the Leaf Area Index (e.g., Begue and Myneni 1996), as well as to vegetation phenology (Moulin et al. 1997), and is often used as a proxy for vegetation activity. In addition, the precipitation rate is analyzed. It is obtained from the Global Precipitation Climatology Product (GPCP) from merged infrared and microwave satellite data and gauge measurements (Huffman et al. 1997). Figure 6 shows the 8-yr time series of normalized values (subtracting the mean and dividing by the standard deviation) of the emissivity polarization difference at 19 GHz, the AVHRR NDVI, and the GPCP rain rate for two locations along the previous transect at 7° and at 13°N. Note that the difference in emissivity between horizontal and vertical polarization is presented, not the opposite as usual, in order to have a positive correlation with the other variables and an easier comparison; an increase in vegetation will thus lead to a decrease in the emissivity polarization difference (in absolute value) and an increase in soil moisture will translate into an increase in the emissivity polarization difference (again in absolute value). For both time series in Fig. 6, the three signals are rather well in phase and the relative amplitudes of the signals from one year to the other are in good agreement (see, e.g., the contrast between 1993 and 1999 in all the signals at 13°N). More precisely, at 13°N, in Chad in a semiarid region, one can observe the following sequence during a year. When it starts raining in the spring (the GPCP rain rate increases), the emissivity polarization difference horizontal minus vertical tends to decrease (this is especially obvious in 1994, 1997, and 1998). This likely means that the soil moisture increases significantly. Then, the emissivity polarization difference horizontal minus vertical (H – V) increases, as a result of the vegetation increase as confirmed by the NDVI variations. One will note the time lag between the precipitation and the vegetation increase as observed with both the NDVI and the microwave emissivity. In a more densely vegetated region

at 7°N and 20°E, the interannual variability of the signal is less obvious and the onsets of precipitation and vegetation activity (as seen by both NDVI and the emissivities) are almost in phase. In conclusion, it appears that in vegetated regions the emissivity difference reacts primarily to the vegetation increase, not to soil moisture variations; in semiarid regions, at the beginning of the rainy season when the vegetation density is very low, the emissivity difference is sensitive to the soil moisture at first, but as soon as the vegetation density increases, the emissivity reacts primarily to the vegetation variability.

However, a rather strong correlation has been found between the passive microwave polarization difference and the soil moisture in some regions, making it possible to retrieve soil moisture from passive microwave observations around 19 GHz. For instance, in Illinois, Vinnikov et al. (1999) found such a good correlation. The role of the vegetation in this correlation has been questioned: is the passive microwave signal strictly related to the soil moisture or is it related to it through a correlation between the vegetation and the soil moisture? This relationship has been examined in detail with SSM/I microwave emissivities in coincidence with in situ soil moisture from a large number of stations (Prigent et al. 2005b) as well as with soil moisture as derived from land surface models (Aires et al. 2005). The passive microwave polarization differences are expected to react in a similar way to an increase of soil moisture or to a decrease in vegetation. As a consequence, in regions where soil moisture and vegetation are anticorrelated (i.e., in midlatitude regions where vegetation density tends to increase in spring and summer when soil moisture decreases) it is difficult to tell to which parameter the passive microwaves are reacting, but when these two variables are positively correlated, it should be possible to separate the two effects. In order to examine these relationships, two years of SSM/I emissivities at 19 GHz over the globe have been analyzed, along with the coincident NDVI observations and the surface soil moisture deduced from the reanalysis of the European Centre for Medium-Range Weather Forecasts (ECMWF). The linear correlation between the microwave emissivities [emissivity polarization difference vertical minus horizontal (V – H) at 19 GHz] and the ECMWF soil moisture is low (–0.27), as is the linear correlation between the same emissivity variable and the NDVI (0.33). Figure 7 shows the linear correlation calculated for each pixel over two years between the emissivity polarization difference at 19 GHz (V – H) and the ECMWF soil moisture versus the linear correlation between the NDVI and
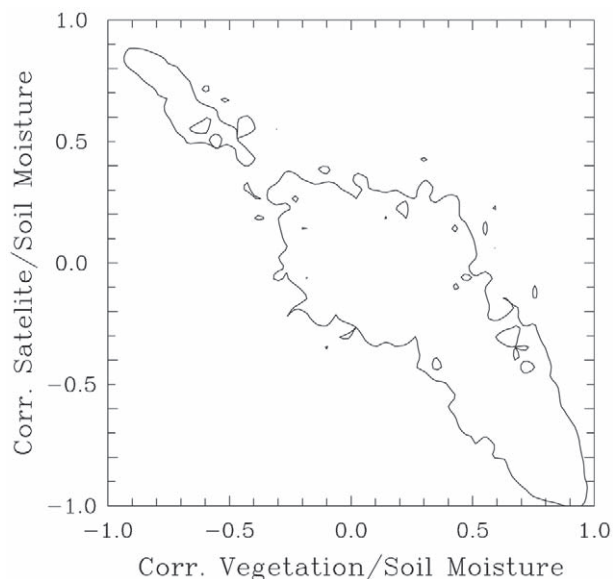

FIG. 7. Population contour (at 0.7%) of the linear correlation between the emissivity polarization difference at 19 GHz (V – H) and the ECMWF soil moisture versus the linear correlation between the NDVI and the ECMWF soil moisture. The correlations are calculated for each pixel on the monthly mean values for 2 yr over snow- and ice-free land surfaces, globally.

the ECMWF soil moisture (also calculated for each pixel over two years). It is clear from this figure that, for each location, the correlation between the passive microwave and the soil moisture, when it exists, is directly related to the correlation between the soil moisture and the vegetation; when the correlation between the vegetation and the soil moisture varies from –1 to 1, the correlation between the emissivity polarization difference and the soil moisture goes from 1 to –1, almost linearly. For more details see Aires et al. (2005).

These analyses emphasize the complex sensitivity of the microwave emissivities to both vegetation and soil moisture. As a consequence, direct and simple retrieval of soil moisture solely from the passive microwave frequency range is unlikely for global application. We developed a methodology that merges multisatellite observations, including passive microwave emissivities, which benefits from the different sensitivity of the different satellite measurements to separate the vegetation and soil moisture contributions (Aires et al. 2005).

Sensitivity of the microwave emissivities to the presence of standing water. Standing water has a high dielectric constant compared to bare dry soil or to vegetation (Giddings and Choudhury 1989; Sippel

et al. 1998). Figure 8 illustrates the microwave emissivities at 37 GHz for both polarizations and for their difference for every other month in 1998 over the Pantanal in Brazil. For a given pixel, the microwave emissivities decline and the polarization differences (V – H) rise with increasing standing water coverage. Over the year, the expansion and contraction of the inundated region is observable. The sensitivity of the microwave emissivities to the inundation has
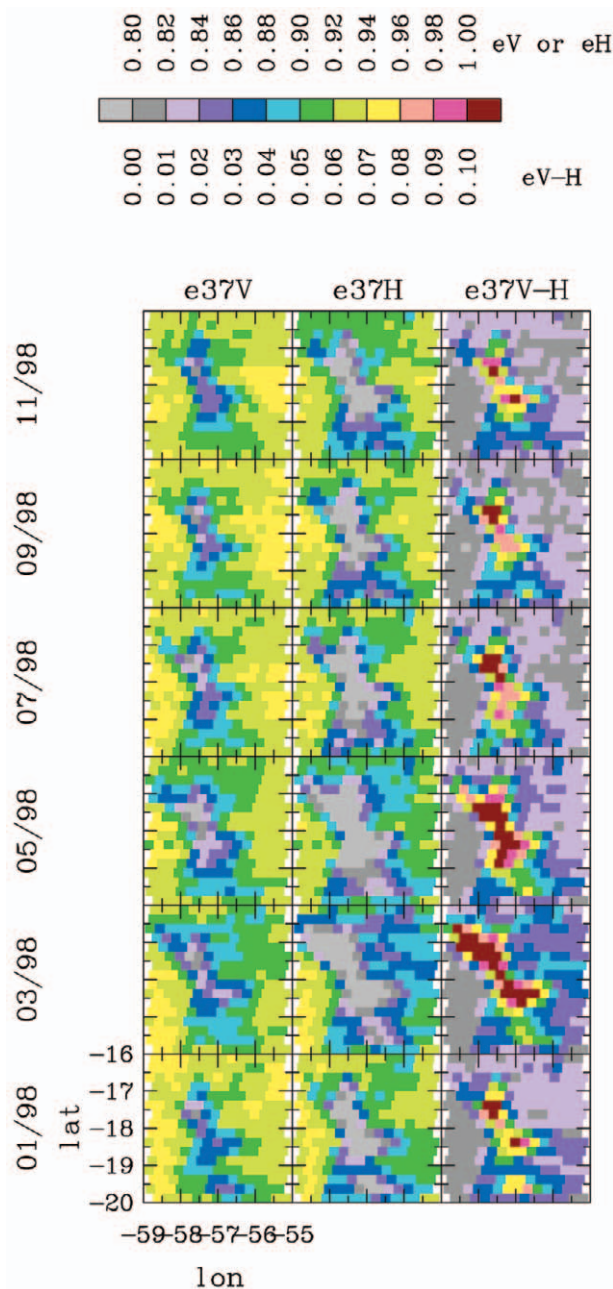
FIG. 8. Microwave emissivities at 37 GHz for both polarizations and for their difference, for every other month in 1998 over the Pantanal in South America.

been exploited to derive global maps of inundation extend and seasonality (Prigent et al. 2001a). In order to qualitatively evaluate the relationship between the microwave emissivities and the presence of water, the time series of the emissivities are compared to the time series of the water-level height derived from the Ocean Topography Experiment (TOPEX)/Poseidon altimeter observations (Fung and Cazenave 2001; Generro et al. 2005). Figure 9 shows this comparison for a specific location over the Pantanal (both variables are normalized as in Fig. 6). There is very good correspondence between the emissivity response and the altimeter signal, confirming the sensitivity of the emissivities to the presence of water.

Sensitivity of the microwave emissivities to snow characteristics. The interaction of the microwave radiation with snow has engendered extensive research. Microwave observations respond to snow properties such as depth, water equivalence, grain size, and embedded or covering vegetation. The magnitude of the responses to these characteristics usually depends upon frequency. With the dielectric losses for ice being small, the extinction coefficient for dry snow is dominated by scattering, this effect being stronger at shorter wavelengths, for larger particles, and drier snow. With increasing wetness, the losses increase and the volume scattering becomes negligible. Wet snowpacks radiate like blackbodies at the physical temperature of the upper snow layer.

Figure 10 shows the microwave emissivities at 19, 37, and 85 GHz (horizontal polarization) for three months during the 1992–93 winter season over North America. The emissivities show considerable variability from one area to another for a given month and from month to month for a given location. For instance, the region north of 50°N is completely covered by snow in January but shows very different responses at all frequencies, from one region to another. Second, for a given region, the satellite observations can undergo significant changes during the winter season, without large variations in the snow cover or snow depth. Ontario in Canada is such a region, with large variations in the emissivity even at 19 GHz during the winter, even though the snow cover does not vary much.
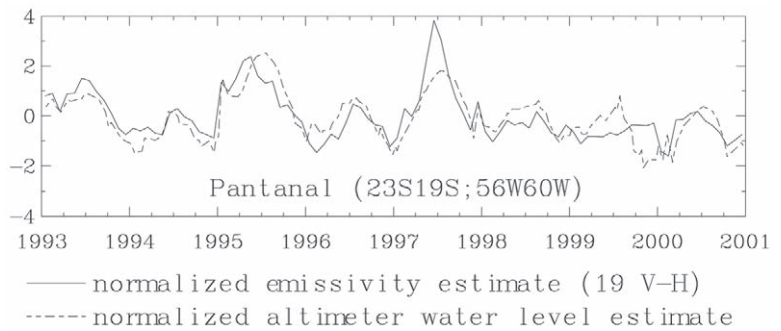
It has been shown that these spatial and temporal variations of the snow responses result from a complex combination of numerous factors, including vegetation, topography, and snow metamorphism during the winter (Cordisco et al. 2006). Taking into account the local statistics limits the signal contamination. The potential for variational assimi-
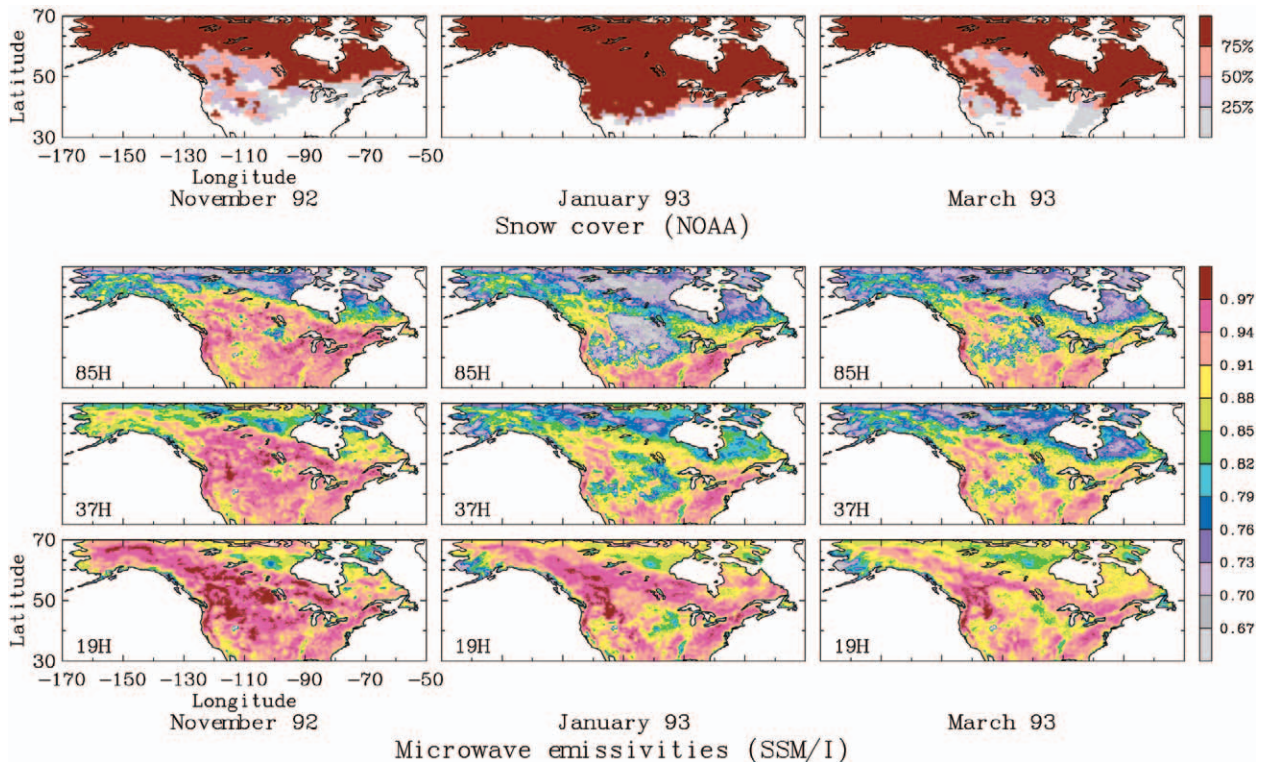
lation of microwave emissivities in the surface model has been quantified. The higher the frequency, the higher the sensitivity to the scattering by larger grains, and thus to snow metamorphism along the winter (Rosenfeld and Grody 2000; Kongoli et al. 2004). The emissivity at 85 GHz is highly sensitive to freshly fallen snow. This frequency has often been avoided in snow detection algorithms, because of its sensitivity to atmospheric changes [e.g., the algorithm derived from the Chang et al. (1987) method]. Using the emissivities instead of the brightness temperatures directly, our preprocessing of the microwave observations (i.e., subtracting the atmospheric contamination) makes it easier to use these frequencies that are very sensitive to both the atmosphere and the presence of snow.

Vegetation and topography also interfere with the signal that is received by the satellite. Comparison with in situ snow depth measurements shows low correlation with the microwave emissivities on a

FIG. 9. The 8-yr time series of normalized values (subtracting the mean and dividing by the std dev) of the emissivity polarization difference at 19 GHz and the water-level height derived from the TOPEX/Poseidon altimeter observations, for a specific location over the Pantanal in South America.

global basis. As a consequence, snow depth retrieval will be very difficult to retrieve with any accuracy from passive microwave observations on a global basis, confirming previous studies (e.g., Kelly et al. 2003; Grippa et al. 2004). To partly alleviate these difficulties, a scheme has been developed to estimate the snow depth: it combines microwave emissivities, in situ measurements, and land surface models (Cordisco et al. 2006).

FIG. 10. Microwave emissivities at 19, 37, and 85 GHz (horizontal polarization) for three months during the 1992–93 winter season over North America along with the NOAA/NESDIS snow cover products (Romanov et al. 2003).

CONCLUSIONS. Microwave emissivities between 19 and 85 GHz have been directly calculated from SSM/I satellite observations, by removing the atmospheric contribution and the surface temperature modulation, using ancillary observations (e.g., the ISCCP dataset and NCEP reanalysis). The calculation method is very generic in nature and can be applied to other microwave imagers and profilers. It has already been applied to AMSU observations (Prigent et al. 2005a; Karbou et al. 2005a) and there is work in progress using the AMSR observations. Limitations have been pointed out, for example, the problem of effective emitting temperature at lower frequencies or the characterization of the uncertainties.

Close to 10 years of monthly mean land surface emissivities are presented in this study at a global scale with a 0.25° × 0.25° spatial resolution. The monthly mean emissivities are available online at http://geo.obspm.fr. Various studies related to these emissivities are described at this Web site.

The uses of these microwave emissivity retrievals are manifold.

First, these emissivities can help characterize the land surface properties. They have been shown to be sensitive to vegetation, soil moisture, the presence of standing water, and snow characteristics. Although the interactions between various sources of variability and the microwave radiation are complex, the passive microwave observations can be exploited along with other satellite measurements of the surface at other wavelengths to estimate land surface properties. Applications include vegetation analysis (Prigent et al. 2001b), estimation of the extent and seasonality of wetlands (Prigent et al. 2001a), and snow characterization (Cordisco et al. 2006). Because the emissivity estimates have been available over a decade at a global scale, it is now possible to analyze the interannual variability of these land properties.

Second, with the emissivity estimates presented in this study, one can calculate the surface contribution to the radiance measured from satellites and, as a consequence, even deduce the atmospheric characteristics from passive microwave over land. Pionner works by Yeh and Liou (1983) and Jones and Vonder Haar (1990) estimated cloud liquid water over land from combined IR and microwave observations. Exploiting the passive microwave observations over land for atmospheric retrievals is now a key challenge for NWP centers where observations from AMSU or SSM/I are still often disregarded over land. For instance, the utilization of microwave sounding observations is usually limited to mid- and upper-tropospheric sounding channels. This emissivity database can provide the necessary statistics (e.g., mean emissivities and emissivity cross correlations between frequencies) for the retrieval of atmospheric parameters over land. Using it, we developed a neural network methodology to retrieve the surface skin temperature, the integrated water vapor content, the cloud liquid water path, and the microwave land surface emissivities between 19 and 85 GHz from SSM/I observations (Aires et al. 2001). A similar method has also been implemented to estimate water vapor and temperature profiles over land with AMSU-A and -B observations (Karbou et al. 2005b). Work has also been performed at ECMWF to use the emissivity values within the specific context and constraint of operational assimilation (Prigent et al. 2005a).

Last, this dataset can help evaluate emissivity models at global scales. Modeling studies are very important to understand the complex interaction between the land surface and the microwave radiation. However, they show limitations when used at the large scale, due to the models themselves and to the uncertainty in the input parameters. Local radiometric measurements can help tune models for specific conditions but they have difficulties capturing and representing the larger-scale components. Analysis of the satellite-derived emissivity is complementary to these studies. Comparison of microwave observations at the global scale can help disentangle the complex interaction between the surface and radiation.

REFERENCES

Aires, F., C. Prigent, W. B. Rossow, and M. Rothstein, 2001: A new neural network approach including first-guess for retrieval of atmospheric water vapor, cloud liquid water path, surface temperature and emissivities over land from satellite microwave observations. *J. Geophys. Res.,* **106,** 14 887–14 907.

——, ——, and ——, 2005: Sensitivity of microwave and infrared satellite observations to soil moisture at a global scale. II: Global statistical relationships. *J. Geophys. Res.,* **110,** D11103, doi:10.1029/2004JD005094.

Begue, A., and R. Myneni, 1996: Operational relationships between NOAA-Advanced Very High Resolution Radiometer vegetation indices and daily fraction of absorbed photosynthetically active radiation, established for Sahelian vegetation canopies. *J. Geophys. Res.,* **101,** 21 275–21 289.

Chang, A. T. C., J. L. Foster, and D. K. Hall, 1987: *Nimbus-7* SSMR derived global snow cover parameters. *Ann. Glaciol.,* **9,** 39–44.

Choudhury, J., 1990: A comparative analysis of satellite-observed visible reflectance and 37 GHz polarization difference to assess land surface change over the Sahel zone. *Climatic Change,* **17,** 193–208.

Colton, M. C., and G. A. Poe, 1999: Intersensor calibration of DMSP SSM/I's: F-8 to F-14, 1987–1997. *IEEE Trans. Geosci. Remote Sens.,* **37,** 418–439.

Cordisco, E., C. Prigent, and F. Aires, 2006: Snow characterization at a global scale with passive microwave satellite observatioons. *J. Geophys. Res.,* in press.

de Ridder, K., 2003: Surface soil moisture monitoring over Europe using Special Sensor Microwave/Imager (SSM/I) imagery. *J. Geophys. Res.,* **108,** 4422, doi:10.1029/2002JD002796.

Fung, L. L., and A. Cazenave, 2001: *Satellite Altimetry and Earth Sciences: A Handbook of Techniques and Applications.* Academic Press, 463 pp.

Gennero, M. C., J.-F. Cretaux, C. Maheu, K. Do Minh, S. Calmant, and A. Cazenave, cited 2005: Surface water monitoring by satellite altimetry. [Available online at www.legos.obs-mip.fr/soa/hydrologie/hydroweb/.]

Giddings, L., and B. J. Choudhury, 1989: Observation of hydrological feature with *Nimbus*-7 37 GHz data applied to South America. *Int. J. Remote Sens.,* **10,** 1673–1686.

Grippa, E., N. Mognard, T. Le Thoan, and E. Josberger, 2004: Siberia snow depth climatology derived from SSM/I data using a combined dynamic and static algorithm. *Remote Sens. Environ.,* **93,** 30–41.

Hewison, T. J., 2001: Airborne measurements of forest and agricultural land surface emissivity at millimeter wavelengths. *IEEE Trans. Geosci. Remote Sens.,* **39,** 393–399.

Huffman, G. J., and Coauthors, 1997: The Global Precipitation Climatology Project (GPCP) combined precipitation dataset. *Bull. Amer. Meteor. Soc.,* **78,** 5–20.

Jones, A. S., and T. H. Vonder Haar, 1990: Passive microwave remote sensing of cloud liquid water over land regions. *J. Geophys. Res.,* **95,** 16 637–16 683.

——, T. Vukicevic, and T. H. Vonder Haar, 2004: A microwave satellite observational operator for variational assimilation of soil moisture. *J. Hydrometeor.,* **5,** 213–229.

Kalnay, E., and Coauthors, 1996: The NCEP/NCAR 40-Year Reanalysis Project. *Bull. Amer. Meteor. Soc.,* **77,** 437–470.

Karbou, F., and C. Prigent, 2005: Calculation of microwave land surface emissivity from satellite observations: Validity of the specular approximation over snow-free surfaces? *IEEE Trans. Geosci. Remote Sens. Lett.,* **2,** 311–314, doi:10.1109/LGRS.2005.847932.

——, ——, L. Eymard, and J. Pardo, 2005a: Microwave land emissivity calculations using AMSU measurements. *IEEE Trans. Geosci. Remote Sens.,* **43,** 948–959.

——, F. Aires, C. Prigent, and L. Eymard, 2005b: Potential for AMSU-A and -B measurements for atmospheric temperature and humidity profiling over land. *J. Geophys. Res.,* **110,** D07109, doi:10.1029/2004JD005318.

Kelly, R. E., A. T. C. Chang, L. Tsang, and J. Foster, 2003: A prototype AMRS-E global snow area and snow depth algorithm. *IEEE Trans. Geosci. Remote Sens.,* **41,** 230–242.

Kongoli, C., N. C. Grody, and R. R. Ferraro, 2004: Interpretation of AMSU microwave measurements for the retrievals of snow water equivalent and snow depth. *J. Geophys. Res.,* **109,** D24111, doi:10.1029/2004JD004836.

Lakshmi, V., E. F. Wood, and B. J. Choudhury, 1997: A soil–canopy–atmosphere model for use in satellite microwave remote sensing. *J. Geophys. Res.,* **102,** 6911–6927.

Matzler, C., 2005: On the determination of surface emissivity from satellite observations. *IEEE Trans. Geosci. Remote Sens. Lett.,* **2,** 160–163, doi:10.1109/LGRS.2004.842448.

Moulin, S., L. Kergoat, N. Viovy, and G. Dedieu, 1997: Global-scale assessment of vegetation phenology using NOAA/AVHRR satellite measurements. *J. Climate,* **10,** 1154–1170.

Owe, M., R. de Jeu, and J. Walker, 2001: A methodology for surface soil moisture and vegetation depth retrieval using the microwave polarization difference index. *IEEE Trans. Geosci. Remote Sens.,* **39,** 1643–1654.

Pellerin, T., J.-P. Wigneron, J.-C. Calvet, and P. Waldteufel, 2003: Global soil moisture retrieval from a synthetic L-band brightness temperature data set. *J. Geophys. Res.,* **108,** 4364, doi:10.1029/2002JD003086.

Prigent, C., W. B. Rossow, and E. Matthews, 1997: Microwave land surface emissivities estimated from SSM/I observations. *J. Geophys. Res.,* **102,** 21 867–21 890.

—, —, and —, 1998: Global maps of microwave land surface emissivities: Potential for land surface characterization. *Radio Sci.,* **33,** 745–751.

—, —, —, and B. Marticorena, 1999: Microwave radiometric signatures of different surface types in deserts. *J. Geophys. Res.,* **104,** 12 147–12 158.

—, J. P. Wigneron, W. B. Rossow, and J. R. Pardo-Carrion, 2000: Frequency and angular variations of land surface microwave emissivities: Can we estimate SSM/T and AMSU emissivities from SSM/I emissivities? *IEEE Trans. Geosci. Remote Sens.,* **38,** 2373–2386.

—, E. Matthews, F. Aires, and W. B. Rossow, 2001a: Remote sensing of global wetland dynamics with multiple satellite data sets. *Geophys. Res. Lett.,* **28,** 4631–4634.

—, F. Aires, W. B. Rossow, and E. Matthews, 2001b: Joint characterization of vegetation by satellite observations from visible to microwave wavelength: A sensitivity analysis. *J. Geophys. Res.,* **106,** 20 665–20 685.

—, F. Chevallier, F. Karbou, P. Bauer, and G. Kelly, 2005a: AMSU-A land surface emissivity estimation for numerical weather prediction assimilation schemes. *J. Appl. Meteor.,* **44,** 416–426.

—, F. Aires, W. B. Rossow, and A. Robock, 2005b: Sensitivity of microwave and infrared satellite observations to soil moisture at a global scale. I: Satellite observations and their relationship to in situ soil moisture measurements. *J. Geophys. Res.,* **110,** D07110, doi:10.1029/2004JD005087.

Rodell, M., and Coauthors, 2004: The Global Land Data Assimilation System. *Bull. Amer. Meteor. Soc.,* **85,** 381–394.

Romanov, P., D. Tarpley, G. Gutman, and T. Carroll, 2003: Mapping and monitoring of the snow cover fraction over North America. *J. Geophys. Res.,* **108,** 8619, doi:10.1029/2002JD003142.

Rosenfeld, S., and N. Grody, 2000: Anomalous spectra of snow cover observed from Special Sensor Microwave/Imager measurements. *J. Geophys. Res.,* **105,** 14 913–14 925.

Rossow, W. B., and R. A. Schiffer, 1999: Advances in understanding clouds from ISCCP. *Bull. Amer. Meteor. Soc.,* **80,** 2261–2287.

Ruston, B. C., and T. H. Vonder Haar, 2004: Characterization of summertime microwave emissivities from the Special Sensor Microwave Imager over the conterminous United States. *J. Geophys. Res.,* **109,** D19103, doi:10.1029/2004JD004890.

Shi, J., K. S. Chen, Q. Lin, T. J. Jackson, P. E. O'Neill, and L. Tsang, 2002: A parameterized surface reflectivity model and estimation of bare-surface soil moisture with L-band radiometers. *IEEE Trans. Geosci. Remote Sens.,* **40,** 2674–2686.

Sippel, S. J., S. K. Hamilton, J. M. Melack, and E. M. Novo, 1998: Passive microwave observations of inundation area and area/stage relation in the Amazon river floodplain. *Int. J. Remote Sens.,* **19,** 3055–3074.

Vinnikov, K. Y., A. Robock, S. Qiu, J. K. Entin, M. Owe, B. J. Choudhury, S. E. Hollinger, and E. G. Njoku, 1999: Satellite remote sensing of soil moisture in Illinois, United States. *J. Geophys. Res.,* **104,** 4145–4168.

Weng, F., B. Yan, and N. C. Grody, 2001: A microwave land emissivity model. *J. Geophys. Res.,* **106,** 20 115–20 123.

Wigneron, J.-P., D. Guyon, J.-C. Calvet, G. Courrier, and N. Bruguier, 1997: Monitoring coniferous forest characteristics using a multifrequency (5–90 GHz) microwave radiometer. *Remote Sens. Environ.,* **60,** 299–310.

Yeh, H. Y., and K. N. Liou, 1983: Remote sounding of cloud parameters from a combination of infrared and microwave channels. *J. Climate Appl. Meteor.,* **22,** 201–213.